Modelling, characterisation and force tracking control of a magnetorheological damper under harmonic excitation

Ubaidillah*

Mechanical Engineering Department,
Faculty of Engineering, Universitas Sebelas Maret (UNS),
Jl. Ir. Sutami 36 A Kentingan Surakarta 57126, Indonesia
E-mail: ubaid.ubaidillah@gmail.com

Khisbullah Hudha and
Faizul Akmar Abd. Kadir

Smart Material and Automotive Control (SMAC) Research Group,
Faculty of Mechanical Engineering,
Universiti Teknikal Malaysia Melaka (UTeM),
Ayer Keroh, 75450 Melaka, Malaysia
E-mail: khisbullah@utem.edu.my
E-mail: faizul@utem.edu.my
*Corresponding author

Abstract: The objective of this paper is to study the performance of a sixth order polynomial approach to model hysteresis behaviour of a magnetorheological (MR) damper under harmonic excitations. The polynomial model is developed based on curve fitting from the experimental results and consists of a pair subsystem namely positive and negative acceleration which correspond to the upper and lower curves. The performance of the proposed polynomial model is compared with a well known non-parametric technique namely inverse model. The energy dissipated and equivalent damping coefficient of the MR damper in terms of input current and displacement amplitude are investigated. From the simulation results, the sixth order polynomial model shows better performance in describing non-linear hysteresis behaviour of the MR damper compared with inverse model. The force tracking control in both simulation and experimental studies demonstrate that a close-loop PI control has the ability to track the desired damping force well.

Keywords: magnetorheological damper; polynomial model; non-parametric technique; hysteresis behaviour; harmonic excitation; force tracking control.

Reference to this paper should be made as follows: Ubaidillah, Hudha, K. and Kadir, F.A.A. (2011) 'Modelling, characterisation and force tracking control of a magnetorheological damper under harmonic excitation', *Int. J. Modelling, Identification and Control*, Vol. 13, Nos. 1/2, pp.9–21.

Biographical notes: Ubaidillah received his BEng in Mechanical Engineering from the Institut Teknologi Sepuluh Nopember (ITS) Surabaya, Indonesia. Currently, he is a Research Assistant and Master student at the Autotronic Laboratory, Faculty of Mechanical Engineering, Universiti Teknikal Malaysia Melaka (UTeM). His research project lies on magnetorheological fluid devices such as MR damper, MR brake and MR engine mounting for vehicle application. His research interests include modelling, identification and control of MR based actuator.

Khisbullah Hudha received his BEng in Mechanical Design from the Bandung Institute of Technology (ITB) Indonesia; MSc from the Department of Engineering Production Design, Technische Hoogeschool Utrecht, the Netherlands; and his PhD on Intelligent Vehicle Dynamics Control using magnetorheological damper from the Malaysia University of Technology (UTM). His research interests include modelling, identification and force tracking control of semi-active damper, evaluation of vehicle ride and handling, electronic chassis control system design and intelligent control. He is currently attached with Universiti Teknikal Malaysia Melaka (UTeM).

Faizul Akmar Abdul Kadir received his BEng in Mechanical Engineering (Automotive) from the Universiti Teknologi Malaysia (UTM) and MSc in Automotive Engineering from the Coventry University, UK. His research interests are in vehicle dynamics and control fields. Currently, he is serving as a Lecturer at the Automotive Department, Universiti Teknikal Malaysia Melaka (UTeM).

1 Introduction

One of more promising approaches for controlling automotive suspension systems employs semi-active damping devices (Hong et al., 2002). The semi-active damping control devices are used to minimise response to external disturbances by adjusting the properties of the device with a small amount of power such as direct current battery (Inman, 1994; Tang et al., 2009). Hence, in comparison with active control, semi-active control devices need considerably less power for their operation. Even when no current is sent to semi-active control devices, they still can perform as passive control devices (Jalili, 2002).

Various kinds of semi-active devices are currently available. Among these are semi-active devices that can generate forces from viscous/viscoelastic-plastic fluid (Dyke et al., 1996). Magnetorheological (MR) dampers fall into this category and currently became the subject of many investigations (Simon et al., 2001; Choi et al., 2001; Kamath and Wereley, 1997; Pang et al., 1998; Jansen and Dyke, 1999, 2000). MR dampers contain controllable fluids that can change their properties when exposed to magnetic fields. According to Spencer et al. (1997), innovative work on controllable fluids began in the late 1940s. By controlling the current to an electromagnetic coil inside the piston of the damper, the MR fluid's viscosity can be changed, resulting in continuously variable real-time damping system (Zapateiro et al., 2009).

In the past five years, the uses of MR dampers for semi-active suspension have been successfully implemented in automotive industries. A review of the Porsche Cayenne in April 2003 (Visnic, 2003) stated that Porsche Cayenne's optional adjustable suspension relies on MR dampers using continuous damping control system known as skyhook moniker. The Chevrolet Corvette (Corbett, 2004) and Cadillac XLR (Raynal, 2003) were also the world's first vehicles equipped with magnetic ride control. The magnetic ride control is a magnetic-fluid based real-time damping for automotive suspension system. The system uses four wheel-to-body displacement sensors to measure wheel motion with respect to the road surface and responds by adjusting the shock damping at the speed of approaching one millisecond.

Some previous works on semi-active suspension control using MR dampers can be found in the literatures, using LQR control (Sheng et al., 2004), H∞ control (Du et al., 2005), sliding mode control (Yokoyama et al., 2001; Lam and Liao, 2001), fuzzy logic control (Craft et al., 2003; Rui et al., 2004; Zhang et al., 2004), neural networks (Yiming and Xiangying, 2004; Guo et al., 2004) and skyhook control (Nishimura and Kayama, 2002; Sireteanu et al., 2004). All the previous works have claimed to achieve better ride performance than their respective counterparts. Most of the published works on semi-active suspension control were assessed using numerical simulation and only a few of them were evaluated experimentally.

An MR damper is relatively a recent damping device, in which the magnitude of the resisting force acting upon a mechanical structure can be adjusted in real time (Roschke and Atray, 2002). Adjustment takes place by varying the amount of current passing through wires embedded in the damper. Its characteristics have been studied through both numerical simulation (Dyke et al., 1996; Schurter and Roschke, 2000) and laboratory tests (Dyke et al., 1997, 1999). To evaluate the potential benefits of MR dampers in vibration control applications and to take the full advantage of these devices, it is necessary to develop a model that can accurately describe the behaviour of the MR damper. Both parametric and non-parametric models have been developed to portray the observed behaviour of MR dampers. Spencer et al. (1997) developed a phenomenological parametric model that accurately portrays the response of a MR damper to cyclic and random excitations for both constant and variable magnetic field. Computational intelligent paradigms have also been implemented in MR damper models using fuzzy logic (Schurter et al., 2000), neural network (Butz et al., 1999) and genetic algorithm (Giuclea et al., 2004). In addition, a non-linear hysteretic arctangent model was proposed in Ang et al. (2004).

The contribution of this work is to propose a hysteresis damper model which can be integrated with a control system. In order to achieve the aim, a type of MR damper is tested and its hysteresis behaviour is investigated in both experimental and simulation work. The experimental results are evaluated in terms of the damping force versus piston velocity and the damping force versus piston displacement. A polynomial approach is used to model the MR damper and then compared with the inverse model proposed by Wang et al. (2005). Both methods are in the class of non-parametric techniques. The validated mathematical model derived from the experimental result is used for investigating the hysteretic behaviour under several excitation amplitudes and input currents due to the limitation of the suspension test machine. From the force versus displacement behaviours, the energy dissipated can be observed by calculating the area enclosed by the force versus displacement graphs. On the other hand, the equivalent damping coefficient can be determined from the correlation between energy dissipated, excitation frequency and the amplitude. In addition, the accuracy of the damping force control using the proposed model is demonstrated in both simulation and experimental studies by employing a simple closed-loop PI control. The inner loop control is simulated to check the tracking ability of the MR damper by employing the validated MR damper model under several input functions such as sinusoidal, square, and saw-tooth. The experimental investigation of the force tracking control is conducted under several sinusoidal input frequencies and amplitudes of the desired damping forces.

This paper is organised as follows: The first section discusses some previous works on the use of the MR damper and some techniques on MR damper modelling; the second section describes the experimental works in obtaining the MR damper behaviour in the forms of force-velocity and force displacement characteristics; the third section, explains the algorithm of the proposed

modelling approach; the fourth section shows the simulation results, validation of the model with experimental data, energy dissipated and equivalent damping coefficient analysis; the fifth section describes the force tracking performance of the proposed model in both simulation and experimental results and the last section consists of some discussion and recommendation for future study.

2 MR damper force behaviour

An MR damper is filled with a controllable fluid that contains dispersed micron-sized magnetically polarisable particles. When the fluid is subjected to magnetic field, the particles are arranged in a pattern and the behaviour of the fluid is changed from being linear viscous to semi-solid in milliseconds. By adjusting the current within an allowable range, the resisting force to motion of the MR damper increases or decreases in a non-linear fashion. When various magnitudes and patterns of current are applied to the MR damper, resistance of the damper to motion can be adjusted. A schematic of a typical MR damper is illustrated in Figure 1.

Figure 1 Schematic of an MR damper

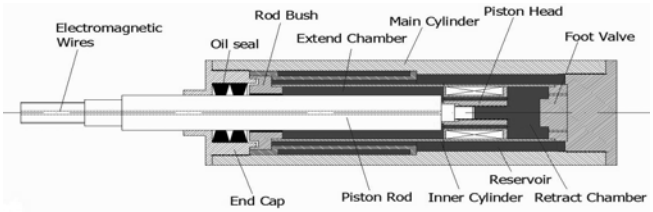

Since the proposed damper model depends on the availability of experimental data, the experimental investigation of force-velocity and force-displacement characteristics of the MR damper needs to be performed. Experiments were set up to obtain the data for identification of the proposed the MR damper model first. Based on the experimental data, a modelling method of the MR damper was realised numerically using a sixth order polynomial equation.

The MR damper used in this study is a magne-ride Delphi, which was manufactured by Delphi Automotive System. The damper consists of a monotube house, piston, magnetic circuit, accumulator, and pressurised gas inside an accumulator and MR fluid. The length of the damper is 48 cm in its extended position and has 8 cm of stroke. The maximum current that can be applied to the electromagnet coils in the magnetic choke is 3.5 amp. and the coil resistance is 1.6 ohm.

The experimental work was carried out in the Autotronic Laboratory, Department of Automotive, Universiti Teknikal Malaysia Melaka (UTeM) using a shock absorber test machine developed by the Smart Material and Automotive Control Group, UTeM. The shock absorber test machine consists of a wire transducer to measure the relative displacement and relative velocity of the damper and load cell to measure the damper force. The integrated measurement and control (IMC) device provides signal processing of the transducers and excitation signals of the slider crank actuator system. These signals are digitally processed and stored in a personal computer using FAMOS control software (IMC, 2002). IMC device is connected to the personal computer using NetBEUI protocol (Scholz, 2000). Control signals to the MR damper are converted to analogue signals by the IMC device. Then, the voltage signals are passed through the current driver and sent to the MR damper. The configuration of the shock absorber test machine available in Autotronic Laboratory is shown in Figure 2.

Figure 2 Shock absorber test machine available at Autotronic Laboratory

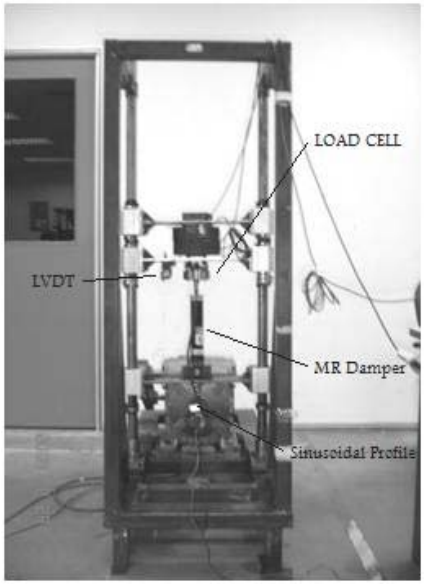

Figure 3 Measured forces for five constant current levels

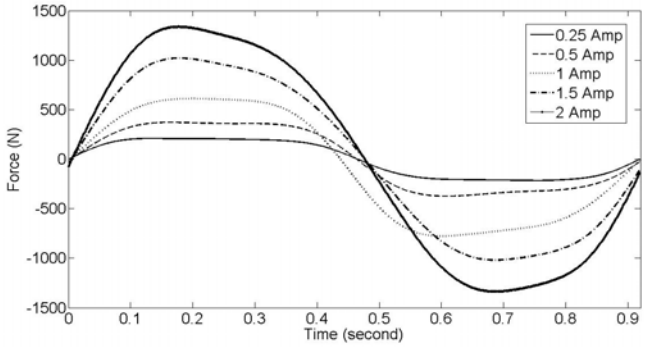

The MR damper testing was done by applying a cyclic motion between the upper and lower ends of the MR damper for different values of applied currents to the damper coils. The response of the MR damper due to 1.08 Hz sinusoidal excitation with amplitude of 2.1 cm was investigated for five constant currents of 0.25, 0.5, 1, 1.5 and 2 amp, being applied by the current driver of the MR damper. The measured forces in time domain, the force-velocity characteristics and the force-displacement characteristics are shown in Figures 3, 4 and 5 respectively. It can be seen from Figures 4 and 5 that the magnitude of

the damping force at the piston velocity and displacement increases proportionally with the increase of the current applied to the damper coils.

Figure 4 Force-velocity characteristic for five constant current levels

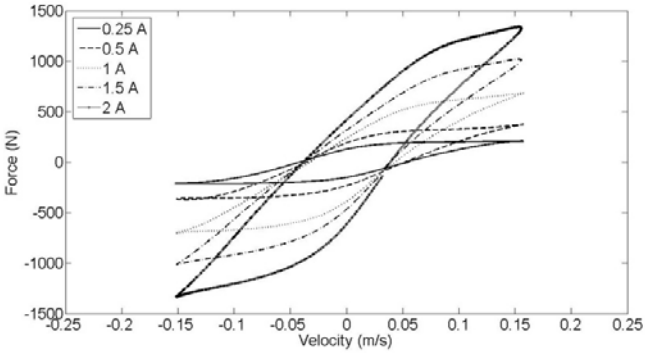

Figure 5 Force-displacement characteristic for five constant current levels

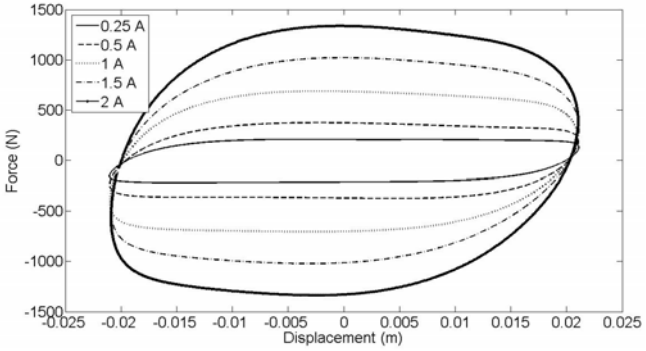

3 MR damper modelling

In this work, two different damper models namely inverse model and sixth order polynomial model are investigated to predict the field-dependent damping force characteristic of the damper. Both models are in a class of non-parametric techniques which employs analytical formulation to describe the characteristics of the device based on both testing data analysis and the MR damper working principle.

3.1 Inverse model

The inverse model of MR damper proposed by Wang et al. (2005) is adopted as a benchmark of the proposed modelling approach in this study. The model describes variations in the damping force as the functions of the control current (i_d), displacement (d_r) and velocity (v_r) of the piston and the nature of the excitation force. The non-linear control current dependence of the damping force is characterised by a non-linear gain based on the asymmetric sigmoid function, while the hysteresis is formulated using a symmetric sigmoid function. The proposed analytical model of symmetric MR-damping force (F_d) is formulated as follows (Wang et al., 2005):

$$f_d = c_i F_h \tag{1}$$

$$c_i = 1 + \frac{k_z}{1+e^{-\alpha_z(i_d+I_0)}} - \frac{k_z}{1+e^{-\alpha_z I_0}}, \quad c_i \geq 1 \tag{2}$$

where c_i is the function of current gain which is equals to 1 when i_d equals to 0. The command current is bounded such that $0 \leq i_d \leq I_m$, where I_m is maximum permissible current that depends upon the design of the damper and the electro-magnetic circuit. F_h represents the passive hysteresis force when i_d equals to 0. Both F_h and c_i are expressed as the functions of I_d, v_r and the seal frictional force F_0 as the following:

$$F_h = F_0 c_e \frac{1-e^{-\alpha(v_r+v_h)}}{1+e^{-\alpha(v_r+v_h)}}\left(1+k_v|v_r|\right) \tag{3}$$

where c_e, k_v, α and v_h are the model parameters which are determined at the maximum damper velocity v_m using the following expressions:

$$c_e = 1 + e^{-\alpha_1 v_m} \tag{4}$$

$$v_m = \sqrt{(\dot{x}_r)^2 - \ddot{x}_r x_r} \tag{5}$$

$$\alpha = \alpha_0 / \left(1 + k_0 v_m\right) \tag{6}$$

$$k_v = k_1 e^{-\alpha_4 v_m} \tag{7}$$

$$v_h = \mathrm{sgn}(\ddot{x}) k_4 v_m + \frac{k_3}{1+e^{-\alpha_3(i_d+I_1)}} - \frac{k_3}{1+e^{-\alpha_3 I_1}} \tag{8}$$

In the above formulations, $\dot{x}_r$ is equal to v_r and the inverse model requires the identification of 13 parameters namely: F_0, I_0, I_1, α_0, α_1, α_2, α_3, α_4, k_0, k_1, k_2, k_3 and k_4 from the measured data (Wang et al., 2005).

3.2 Sixth order polynomial equation model

In order to build an easy-for-implementation MR damper model for both simulation and real-time control systems, the proposed modelling approach is developed based on the experimental data and consists of five main steps. The structure of the proposed MR damper model depicted from Simulink block diagram is shown in Figure 6. In the first step, experimental works on investigating the force-velocity curve of MR damper behaviour are performed for a set of constant values of applied current namely 0.25, 0.5, 1, 1.5, 2 ampere and a cyclic motion of 1.08 Hz. The second step is obtaining the hard points of experimental data from step one as illustrated in Figure 7. The hysteresis loop of each force-velocity curve is divided into two regions namely positive acceleration (upper loop) and negative acceleration (lower loop). Then the third step as proposed by Choi et al. (2001) is fitting both the upper loop and lower loop by the polynomial function expressed as follow;

$$F = \sum_{i=0}^{n} a_i v^i, \quad n = 6 \tag{9}$$

Figure 6 The structure of the 6th order polynomial model

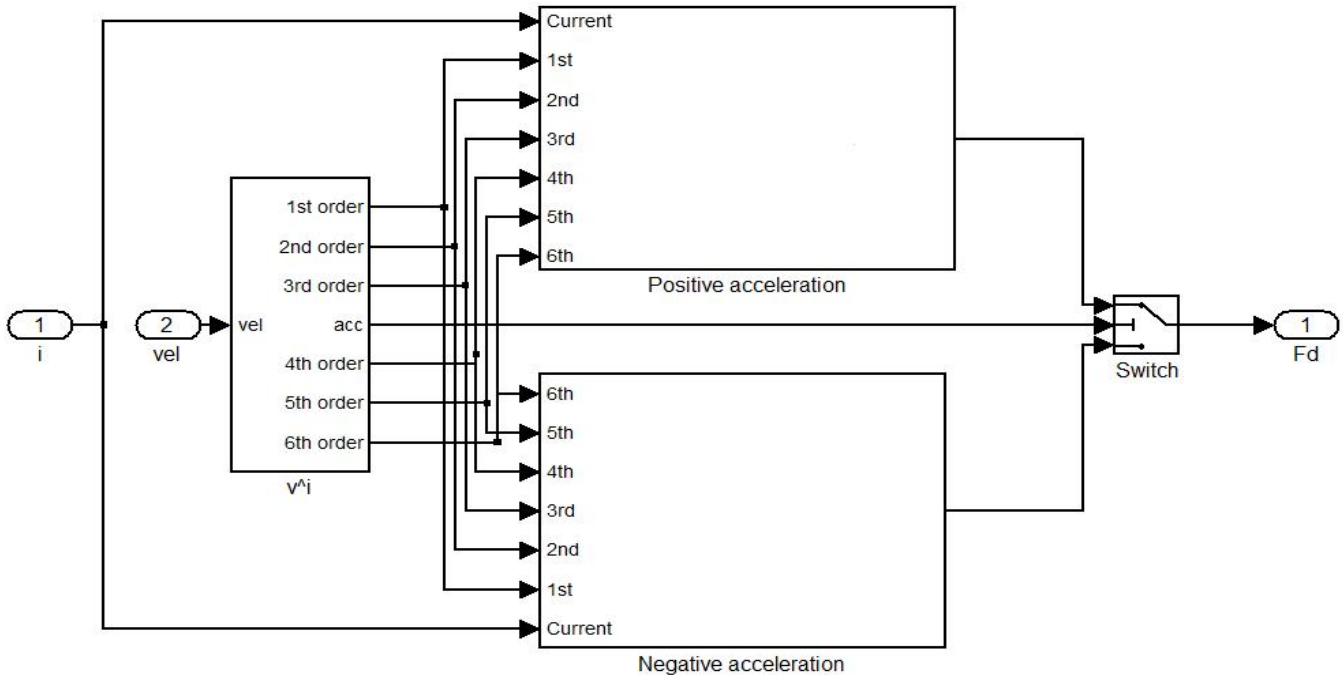

Figure 7 Hard points taken from the experimental result

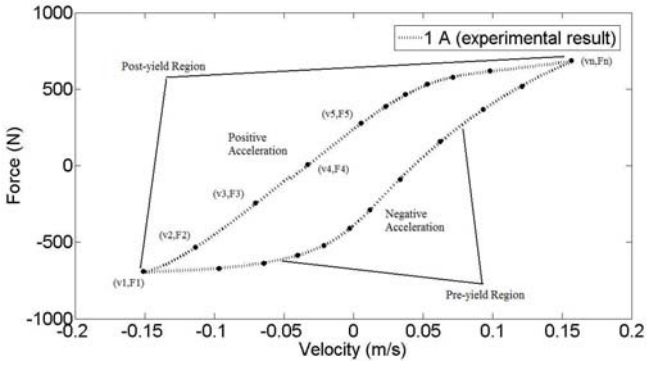

where F is the damper force, a_i is the experimental coefficient to be determined from the curve fitting and v is the damper velocity. In this work, the order of the polynomial for the damping force model is chosen by trial and error. After several investigations, it is observed that 6th order or higher order polynomials are able to capture the hysteresis behaviour of MR damper. Considering computational time and implementation in real-time control of the damper, a 6th order polynomial is selected in this study.

The fourth step is linearisation of the coefficient a_i for each curve. In this step, the coefficient of a_i is linearly approximated with respect to the input current (Choi et al., 2001; Du et al., 2005). The linearisation of the coefficient a_i is governed as follows.

$$a_i = b_i + Ic_i, \quad i = 0,1,2,...,6 \tag{10}$$

After substituting equation (10) into equation (9), the damping force can be expressed as follows,

$$F = \sum_{i=0}^{n} \left(b_i + Ic_i\right) v^i, \quad n = 6 \tag{11}$$

Table 1 Coefficients of the 6th order polynomial model

Negative acceleration			
Parameter	*Value*	*Parameter*	*Value*
b_0	–92,0627	c_0	–260,2950
b_1	864,8735	c_1	5876,2811
b_2	10847,5000	c_2	28450,0000
b_3	3373,7931	c_3	–191522,7586
b_4	–45927,0690	c_4	–1566475,862
b_5	–676829,3103	c_5	4647275,8620
b_6	7033362,0690	c_6	34594827,5900
Positive acceleration			
Parameter	*Value*	*Parameter*	*Value*
b_0	82,9446	c_0	159,3602
b_1	1567,7540	c_1	4551,6440
b_2	–19780,9000	c_2	4957,1190
b_3	–69390,3000	c_3	–26713,4000
b_4	1257495,2590	c_4	–1242506,5520
b_5	1184779,3100	c_5	104524,1379
b_6	–24121551,7200	c_6	31239310,3400

The coefficients of b_i and c_i are obtained from the slope and the intercept of the particular coefficients of the curve fitting. From the investigation, the coefficients of a_i, b_i and c_i are not responsive to the magnitude of the applied current and the direction of relative velocity vector. Therefore, it is easy to realise the close-loop control system to achieve the desired damping force. The values of b_i and c_i used in this study are listed in Table 1.

In the last step, the output of the model namely damper force is selected by a switch block. The switch block will

pass through the output of positive acceleration subsystem if the acceleration of the damper greater or equal to zero. Otherwise, the switch block will pass through the output of negative acceleration subsystem.

4 Model validation

Simulation was performed to explore the validity and the accuracy of the proposed model in MATLAB-Simulink environment. The parameters of the inverse model were created based on minimising the error between the forces predicted by the model (F_d) with the actual force (F_a) obtained experimentally. The objective function, J is given as

$$j = \sum_{i=1}^{n} \left(F_{ai} - F_{di} \right)^2 \tag{12}$$

where n is the total number of experimental data values in one cycle of excitation.

The hard points of the proposed model are obtained from the experimental data. The response of the proposed model is compared to the responses of the inverse model along with the experimental data of force-velocity characteristics as shown in Figure 8. During simulation study, the excitation frequency and magnitude are chosen as 1.08 Hz and ± 0.021m respectively. These parameters are based on the experimental work. From Figure 9, it can be seen that the inverse model and the proposed model are fairly good in predicting the experimental data in post-yield regions. On the other hand, the proposed model shows better performance compared to the inverse model in predicting the behaviour of the experimental data in pre-yield region. From the figure it can be noted that the performance of the proposed MR damper model increases when the input current is increased.

In order to validate the effectiveness of the proposed polynomial model, the input current will be changed. The measured damping force obtained from experimental work and the predicted damping force from the polynomial model are compared as shown in Figures 9(a) and (b), where the excitation frequency and applied current are selected as 1.08 Hz, 0.35 amp. and 0.75 amp., respectively. It is clearly observed that the 6th order polynomial model predicts well the hysteresis behaviour at various input currents. From Figure 9, it can be conclude that the polynomial model can predict the damping force at a certain piston velocity under various conditions without re-optimising the coefficients of a_i, b_i and c_i.

Figure 8 Comparison of the measured and predicted damping forces for: (a) 0.5 amp., (b) 1 amp., (c) 1.5 amp. and (d) 2 amp. applied currents

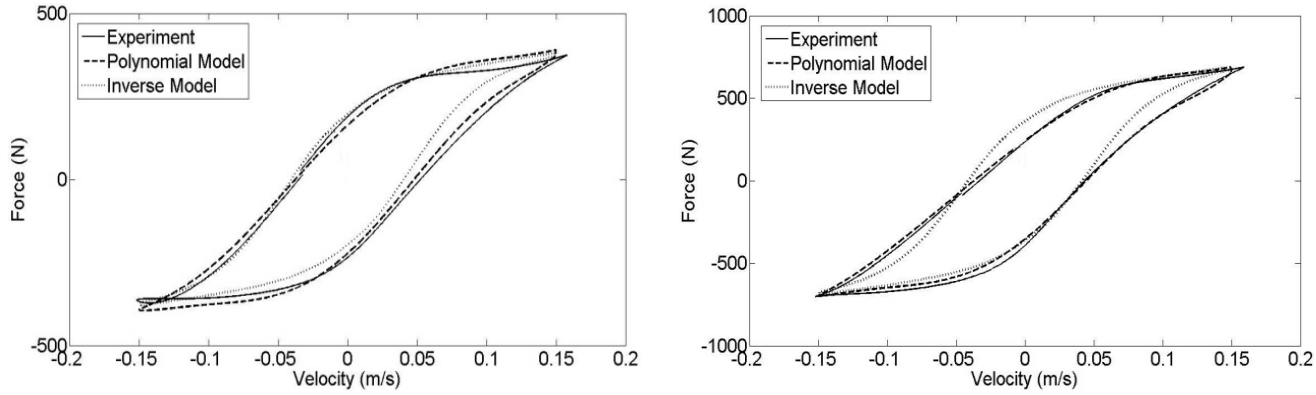

(a)

(b)

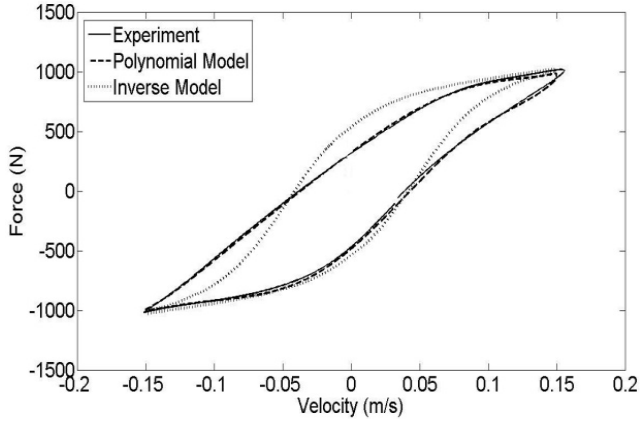

(a)

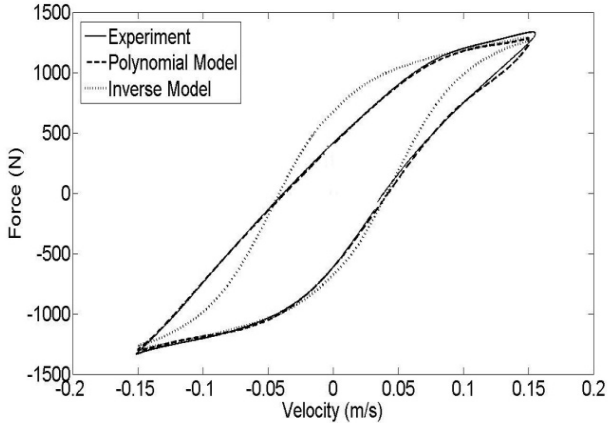

(b)

Figure 9 Damping force characteristics under various input currents: (a) 0.35 amp. and (b) 0.75 amp.

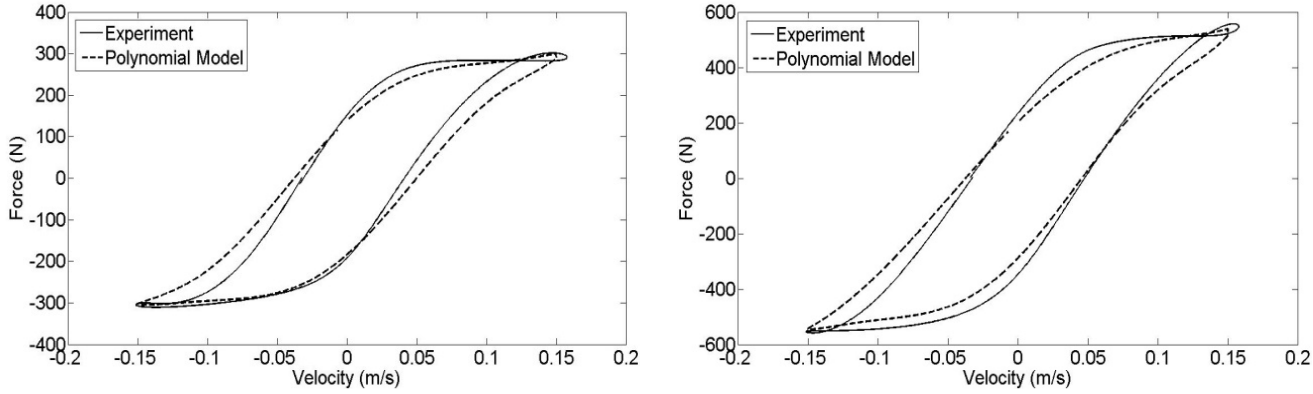

(a) (b)

The overall comparison of force-velocity and force-displacement characteristics under various input currents between experimental data and polynomial model responses are shown in Figures 10 and 11 respectively. From these figures, it can be seen that the proposed polynomial model is able to closely follow the experimental data in both post-yield and pre-yield regions.

Figure 10 Force-velocity characteristics comparison (solid line indicates experimental result and dashed line indicates simulation results)

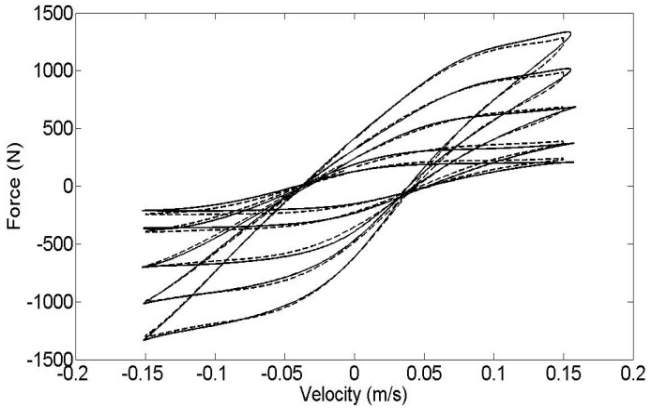

Figure 11 Force-displacement characteristics comparison (solid line indicates experimental result and dashed line indicates simulation results)

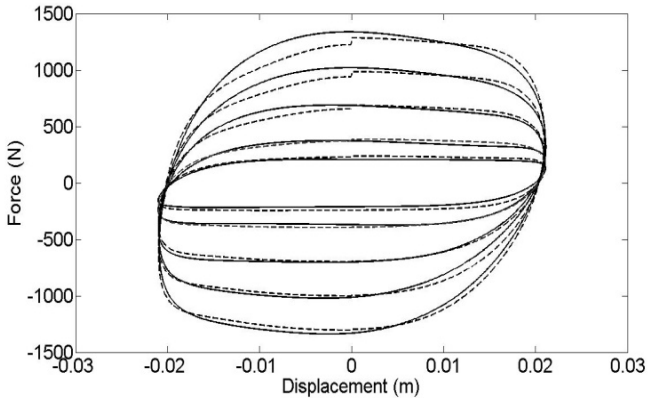

In order to compare the damping performance of the MR damper with the passive viscous damper, it is important to determine the equivalent damping coefficient C_{eq} by equating the energy dissipated in a full cycle (Liao et al., 2003; Wereley et al., 1998). Due to the limitation of the suspension test machine available at Autotronic Laboratory, the sinusoidal excitations with different amplitudes are employed to the validated MR damper model to investigate the characteristics under different constant currents and excitation amplitudes. For example, by applying 0.5 ampere input current, five sets of data (peak amplitudes of excitations are 0.01, 0.02, 0.03, 0.04 and 0.05 m) under the excitation frequency of 1.08 Hz are obtained and both force versus displacement and force versus velocity are shown in Figures 12 and 13 respectively.

The energy dissipated by the MR damper in full cycle can be obtained from the following equation. Let W be the energy dissipated,

$$W_{mr} = \int_0^{2\pi/\omega_d} F_{mr} dx = \int_0^{2\pi/\omega_d} C_{eq} \dot{x} dx \tag{13}$$

where ω_d is the actuation frequency of the sinusoidal excitation, $\dot{x}$ is the relative velocity of the damper and F_{mr} is the damping force.

Figure 12 Force-displacement characteristics with different excitation amplitudes

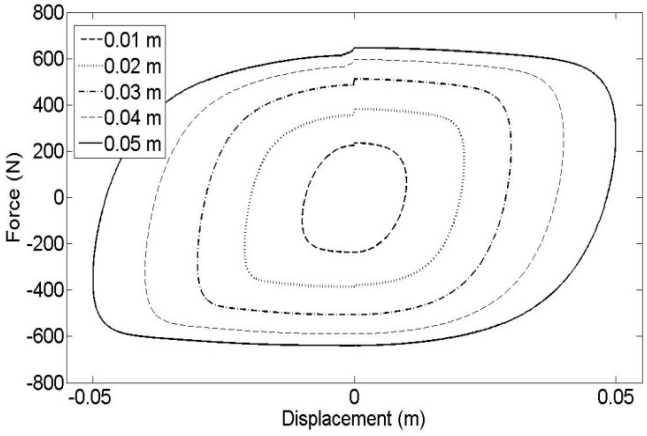

Figure 13 Force-velocity characteristics with different excitation amplitudes

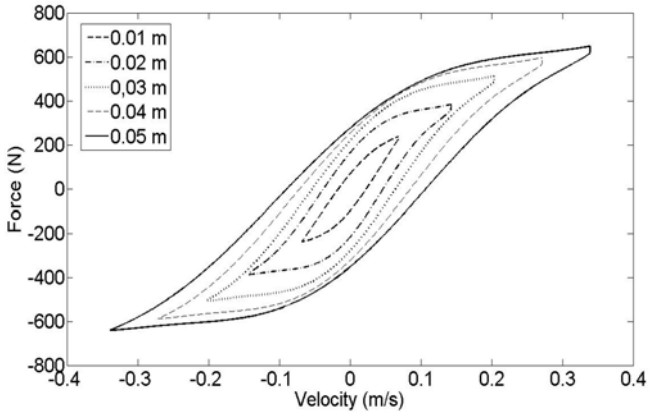

Figure 14 Energy dissipated versus current under various excitation amplitudes

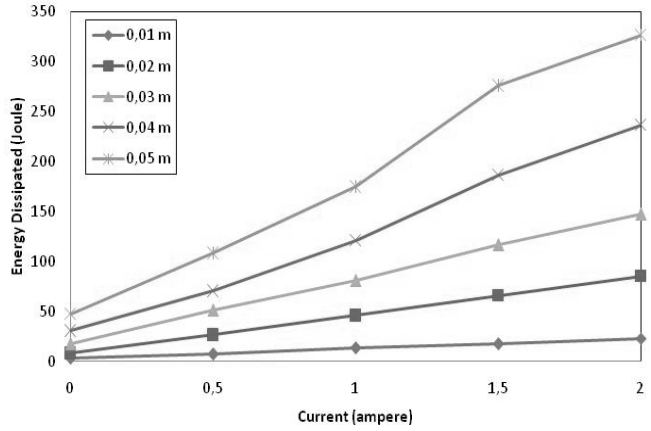

In each case under particular excitation frequency, input current and excitation amplitude, the energy dissipated can be determined by calculating the area enclosed by the curve force versus displacement. Figures 14 and 15 show the relations between energy dissipated, input current and excitation amplitude under a constant excitation frequency of 1.08 Hz. From Figure 14, it can be seen that the greater the excitation amplitude, the greater the energy dissipated, mainly due to a larger hysteresis loop. For higher input current, the loop will be larger due to the higher damping force in which it shows a larger amount of energy dissipated. This result is shown in Figure 15.

Assumed that a simple harmonic excitation, $x = X \sin \omega_d t$, is employed into equation (13) in which X is the excitation amplitude. The equation (13) becomes,

$$\begin{aligned} W_{mr} &= \int_0^{2\pi/\omega_d} C_{eq} \left(\dot{x}\right)^2 dx \\ &= \int_0^{2\pi/\omega_d} C_{eq} \left(\omega_d X \cos \omega_d t\right)^2 dx \\ &= \pi C_{eq} \omega_d X^2 \end{aligned} \tag{14}$$

Therefore, C_{eq} can be formed as

$$C_{eq} = \frac{W_{mr}}{\pi \omega_d X^2} \tag{15}$$

Figure 15 Energy dissipated versus excitation amplitude under various input currents

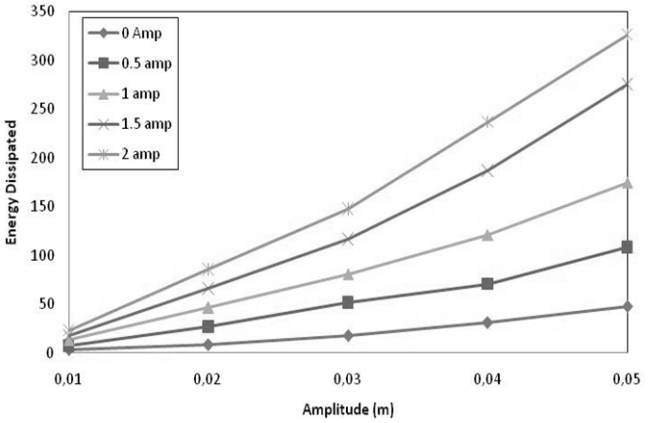

Figure 16 and 17 show the relations among input current, excitation amplitude and equivalent damping coefficient. The damping coefficients in these figures respect to the energy dissipated shown in Figures 14 and 15 respectively. Figure 16 show that the increase of the input current for constant excitation amplitude affects the increase of the damping coefficient. It can be observed that for the amount of increment in equivalent damping coefficient, the effect in the increase of current on low excitation amplitude is more significant than that on the higher excitation amplitude. It can be concluded that the applied current at low excitation amplitude changes the value of equivalent damping coefficient significantly where the piston velocity is relatively low for a fixed frequency. However, for the higher piston velocity when the displacement amplitude is higher, the change in equivalent damping coefficient with the increment of the input current is less considerable. Compared with Figure 14, both of them have the same trend. However, the increment value of equivalent damping coefficient for a certain input current is not significant.

From Figure 17, it can be seen that under the same input current as the increase of the excitation amplitude, the equivalent damping coefficient decreases. Compared with Figure 15, which shows that the energy dissipated increases with the increase of excitation amplitude, it is interesting to observe the trend for equivalent damping coefficient in which it displays an opposite trend in the same input current. This occurrence is caused by the equivalent damping coefficient in equation (14) is treated as a normalised damping coefficient for the amount of energy dissipated with respect to excitation amplitude and frequency. The value of energy dissipated is divided by the square of excitation amplitude so that the graphs display as parabolic function. Therefore, for the linear increment of energy dissipated with the increase of excitation amplitude, the equivalent damping coefficient decrease with the increase of excitation amplitude.

Figure 16 Equivalent damping coefficient versus current under various excitation amplitudes

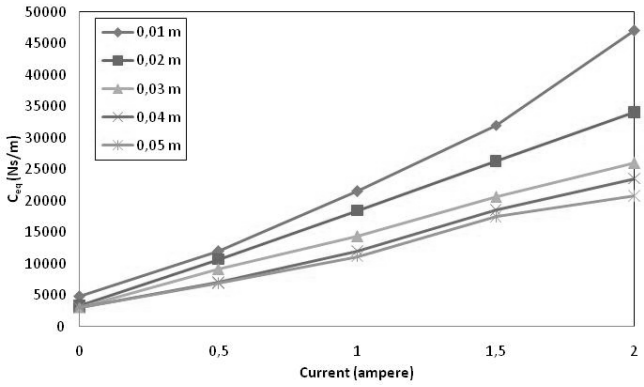

Figure 17 Equivalent damping coefficient versus excitation amplitude under various input currents

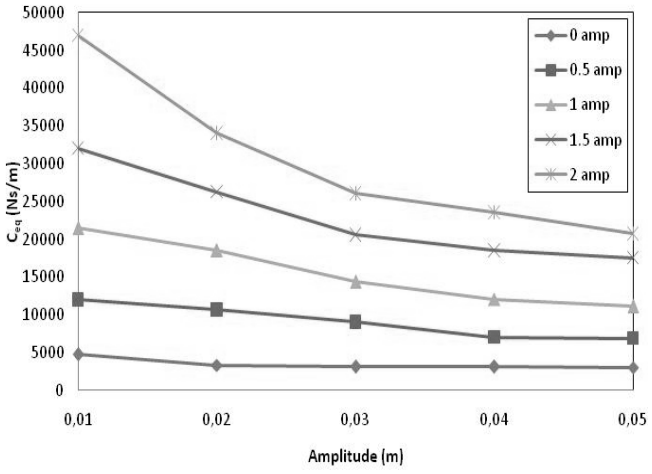

5 Force tracking control of the proposed MR damper model

Besides, having the similar behaviour as the prototype of MR damper, a good MR damper model must be easily controlled. In this section, a force-tracking control of the proposed MR damper model is performed in both simulation study and experimental works. The simulation study is executed in MATLAB-Simulink environment for sinusoidal, square and saw-tooth function of desired force. The structure of force tracking control of the proposed MR damper model using a PI control are shown in Figure 18 which illustrates a closed-loop control system to achieve a desirable damping force. Related with tracking control, the PI or PID has also been used for another application such as personal robot tracking system (Goodhew et al., 2006). The PI controller is formulated as follows,

$$u(t) = K_p e(t) + K_i \int e(t) \tag{16}$$

$$e(t) = F_d(t) - F_a(t) \tag{17}$$

where F_d is the desired damping force and F_a is the actual damping force. In this simulation study, the parameters of K_p and K_i were chosen by trial and error method, where the values of K_p and K_i are set to 0.00769 and 0.000769 respectively. The simulation results under various functions of desired force are shown in Figure 19. Force tracking control is intended to check the tracking ability of the force tracking controller for a class of continuous and discontinuous functions. It is well known that the simulation results show the damping force controllability realised from the close-loop controller. From Figure 19, it can be concluded that the sixth order polynomial model of MR damper has a good capability in tracking the desired force in the whole range of the piston velocity.

Although the simulation study was conducted using validated MR damper model, it is important to conduct the experimental work on force tracking control of MR damper. In this study, the experimental work was conducted using suspension test machine using sinusoidal input at the excitation frequency of 0.7 Hz, 1.08 Hz and 1.5 Hz and the excitation amplitude of 0.021 m. The experimental results of force tracking control for the excitation frequency of 0.7 Hz and 1.5 Hz were shown Figure 20 and 21. While Table 2 summarises the RMS values and deviation percentages between the actual and desired forces in 0.7 Hz, 1.08 Hz and 1.5 Hz excitation frequencies.

Figure 18 The structure of force tracking control of MR damper

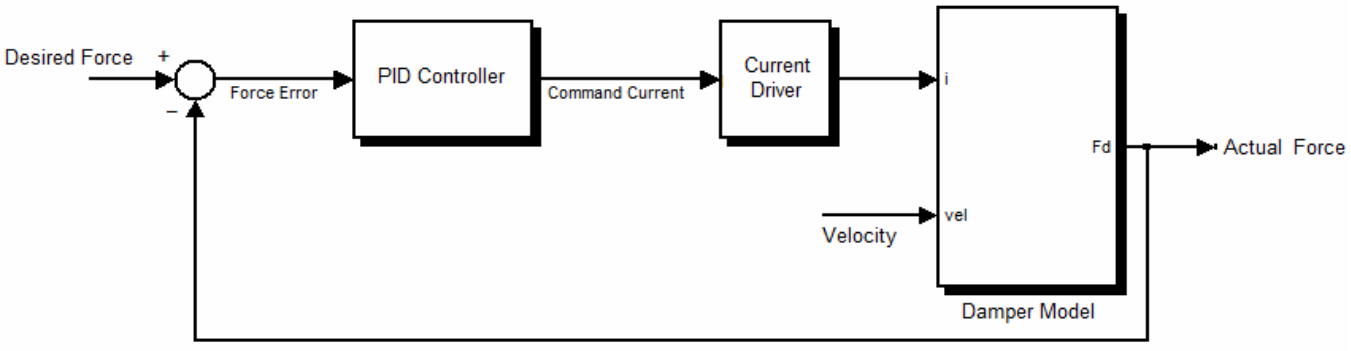

Figure 19 Simulation results of force tracking control at the excitation frequency of 1.5 Hz: (a) sinusoidal, (b) saw-tooth and (c) square

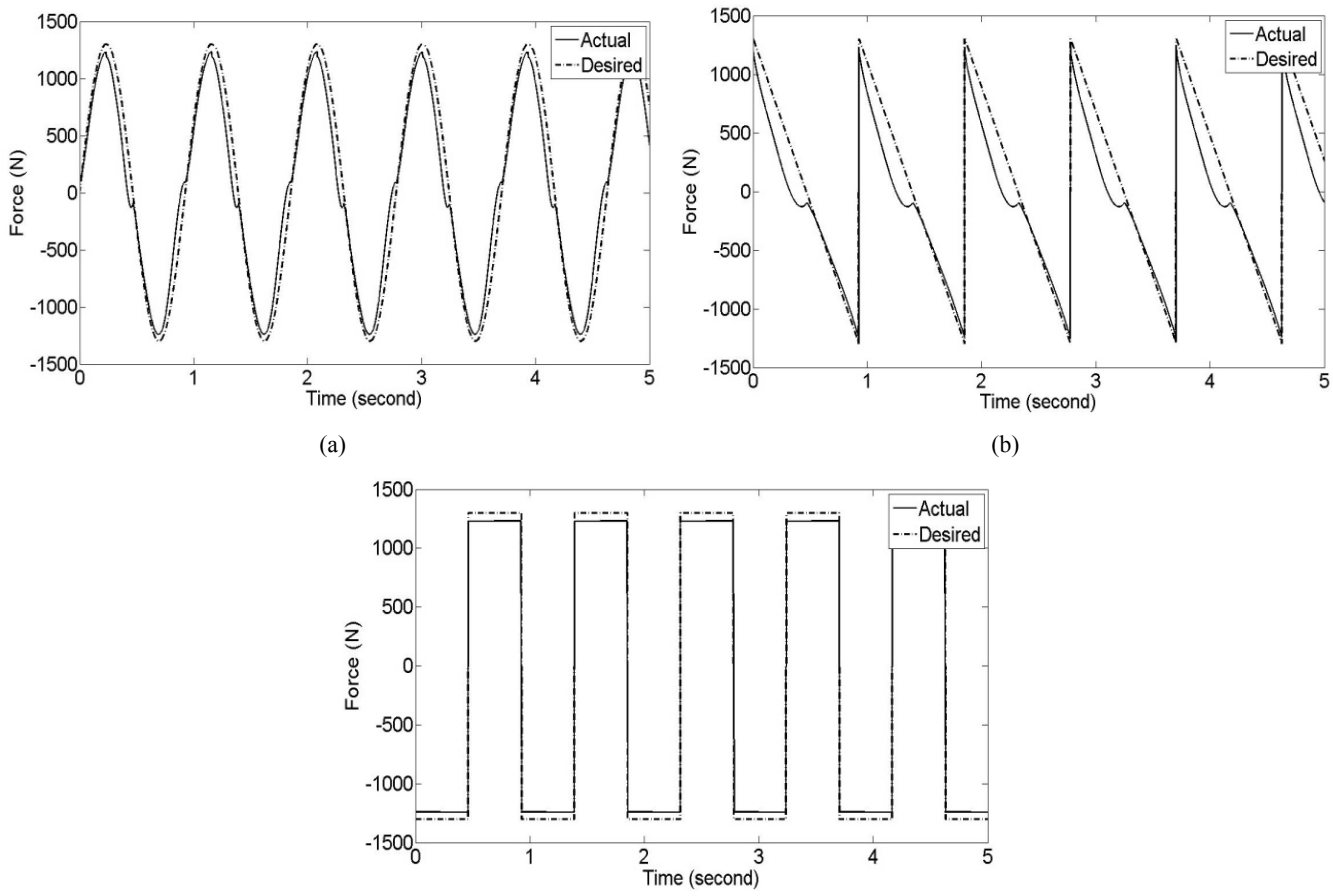

(a) (b)

(c)

Figure 20 The experimental results of force tracking control under several sinusoidal amplitudes of the desired forces at the frequency of 0.7Hz: (a) 500 N, (b) 800 N, (c) 1,100 N and (d) 1,300 N

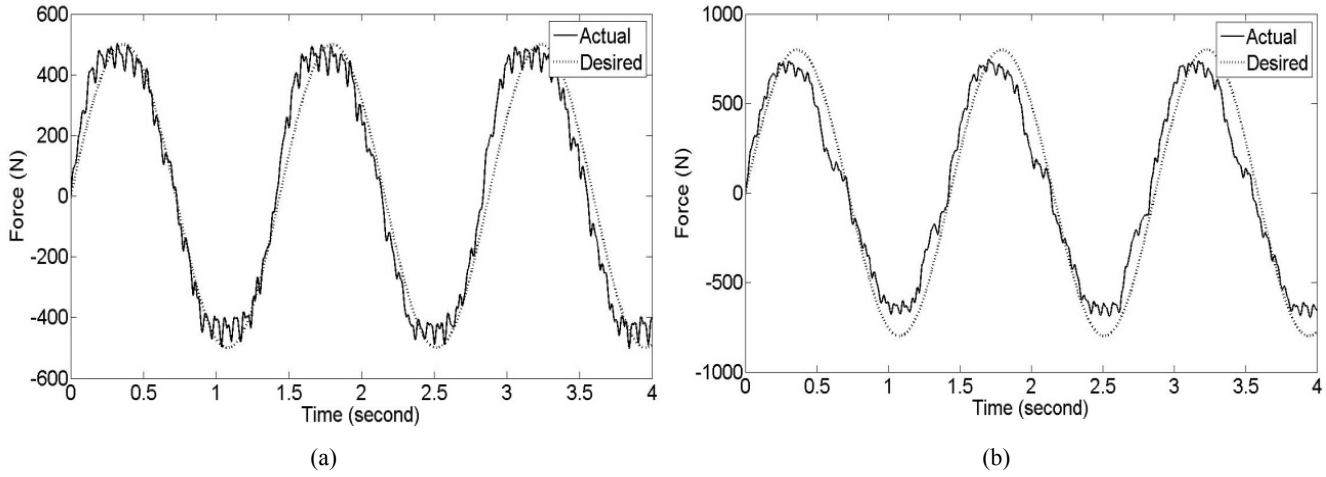

(a) (b)

Figure 20 The experimental results of force tracking control under several sinusoidal amplitudes of the desired forces at the frequency of 0.7Hz: (a) 500 N, (b) 800 N, (c) 1,100 N and (d) 1,300 N (continued)

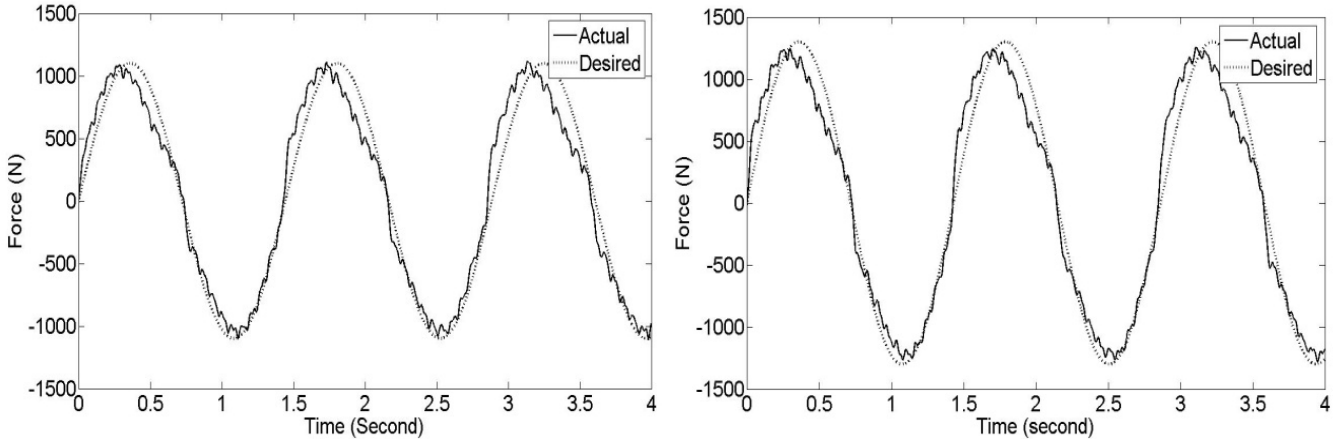

(c) (d)

Figure 21 The experimental results of force tracking control under several sinusoidal amplitudes of the desired forces at the frequency of 1.5Hz: (a) 500 N, (b) 800 N, (c) 1,100 N and (d) 1,300 N

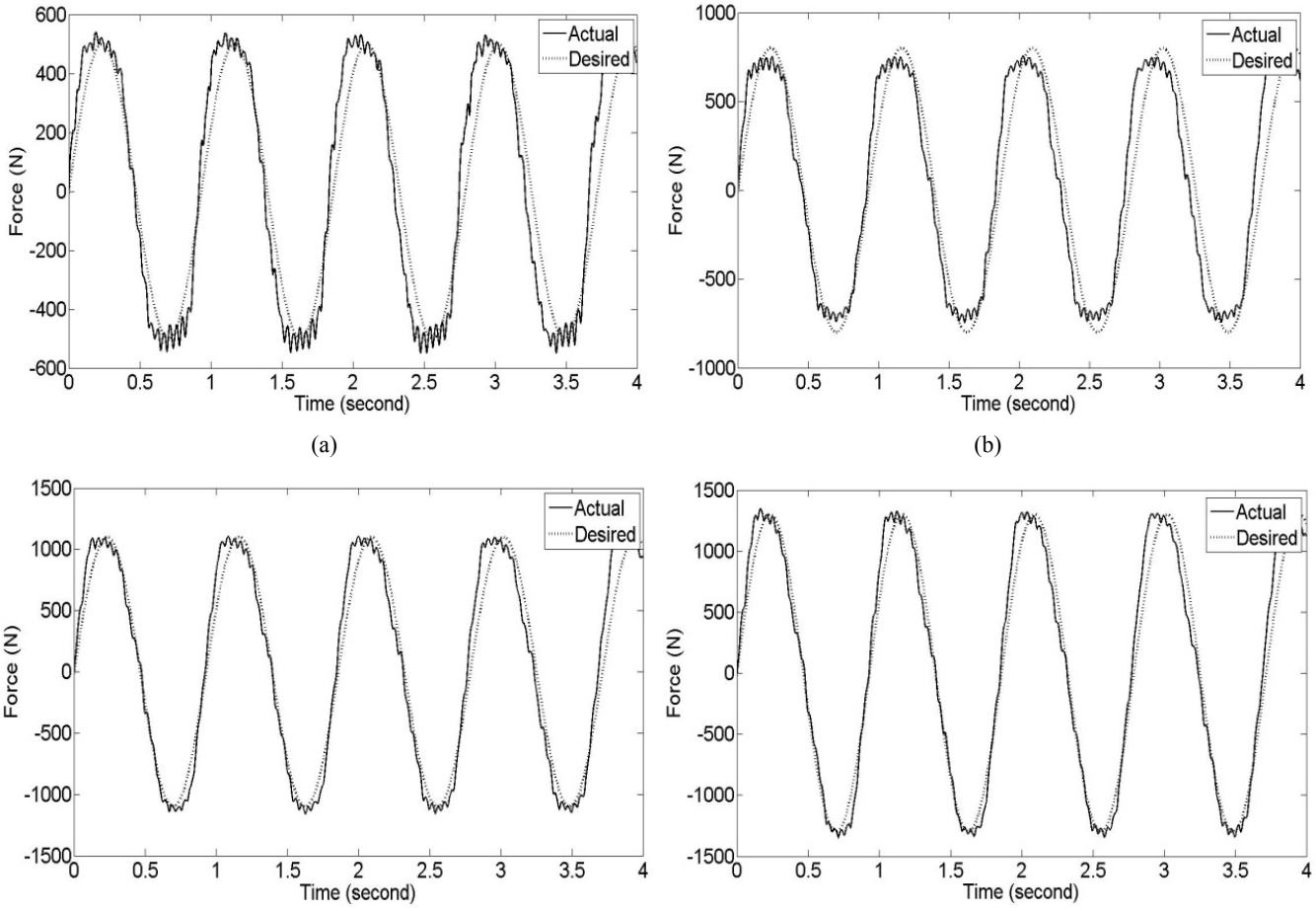

(a) (b)

(c) (d)

Table 2 RMS values and deviation percentages of the force tracking control

Excitation frequency (Hz)	*Peak force (N)*	*Measured force (N)*		*Deviation percentage (%)*
		Desired	*Actual*	
0.7	500	335.3163	356.5362	5.9517
	800	459.1649	493.4251	6.9433
	1,100	778.9565	745.7902	4.4471
	1,300	915.6559	879.5814	4.1013
1.08	500	383.7646	408.8209	6.1289
	800	542.4311	569.6498	4.7781
	1,100	788.7961	755.4405	4.4154
	1,300	926.9724	965.8285	4.0231
1.5	500	380.8582	398.1383	4.3402
	800	556.3194	586.6299	5.1669
	1,100	898.7126	926.9493	3.0462
	1,300	1,020.9465	1,045.7586	2.3726

In experimental work, it is important to note that the output voltage from the controller hardware is in the form of pulse. Using a pulse width modulation signal, the power consumption of MR damper is less than using an analogue signal. The value of voltage applied to the current driver is represented by the width of the generated pulse. The higher the current applied to the MR damper by the current driver, the wider the voltage pulse width generated by the controller hardware to the current driver. From Figure 20 and 21, it can be seen that there is a chattering effect at the peak value of the actual damping force especially for the desired forces of 500N. The chattering effect may be caused by the width of the pulse applied to the current driver in which the lower amplitude of the desired force, the tighter width of the pulse supplied. At the higher desired forces of 800 N, 1,100 N and 1,300 N, the chattering effect reduces significantly.

In terms of the increasing excitation frequency of the experimental work, frequency of control signals generated by the IMC Devices that is too low compared to the working frequency of the PWM hardware will also cause the chattering effect. From these figure, the chattering effect reduces when the applied excitation frequency is added from 0.7 Hz until 1.5 Hz. Generally, the experimental results still can be accepted since the actual damping force could track the desired damping force with small deviation. For all the experimental results, it can be concluded that the PI control can realise the damping force tracking ability under various frequencies and desired forces.

6 Conclusions

The proposed sixth order polynomial model for field-dependent damping force of MR damper has been investigated in this study. The measured experimental damping force was compared with the predicted ones from the inverse model and the proposed model. It has been demonstrated that the proposed model agrees well the non-linear behaviour hysteresis behaviour of the MR damper in the form of force-velocity and force-displacement characteristics. The advantages of the proposed model are in the use of a simple algorithm and do not need a length numerical optimisation for parameter estimation. The energy dissipated and equivalent damping coefficient of the MR damper in terms of input current and excitation amplitude were also investigated. With the increase of excitation amplitude in a certain input current, the energy dissipated has an opposite characteristic with the equivalent damping coefficient in which the energy dissipated is increase and vice versa. In addition, the controllability of the proposed model was investigated in both simulation and experimental works by realising a simple closed-loop control namely PI control. From simulation study, it can be seen clearly that under several input functions, the proposed polynomial model tracks the desired damping force well. To check the performance of the PI control, an experimental work has been performed under various frequencies and desired damping forces. It can be concluded that the PI control shows a good performance in tracking the desired damping force under various conditions by allowing the chattering effect appears at the low actual damping force.

References

Ang, W.L., Li, W.H. and Du, H. (2004) 'Experimental and modeling approach of a MR damper performance under harmonic loading', *Journal of The Institution of Engineers*, Singapore, Vol. 44, No. 4, pp.1–14.

Butz, T. and Stryk, O. (1999) *Modelling and Simulation of Rheological Devices*, Tehnische Universitat Munchen, Universitat Augsburg, Preprint SFB-438-9911.

Choi, S.B., Lee, S.K. and Park, Y.P. (2001) 'A hysteresis model for the field-dependent damping force of a magneto-rheological damper', J*ournal of Sound and Vibration*, Vol. 245, No. 2, pp.375–383.

Corbett, B. (2004) 'Ready for takeoff: a review of the Chevrolet Corvette', *Ward's Auto World Magazine*, October.

Craft, M.J., Buckner, G.D. and Anderson, R.D. (2003) 'Semi-active vehicle shock absorbers: design and experimental evaluations', *Proceedings of SPIE – The International Society for Optical Engineering*, SPIE, March 3–6, San Diego, CA, pp.577–588.

Du, H., Yim, S.K. and Lam, J. (2005) 'Semi-active H∞control of vehicle suspension with magnetorheological dampers', *Journal of Sound and Vibration*, Vol. 283, Nos. 3–5, pp.981–996.

Dyke, S.J., Spencer, B.F., Sain, M.K. and Carlson, J.D. (1996) 'Modeling and control of magneto-rheological dampers for seismic response reduction', Journal of Smart Materials and Structures, Vol. 5, pp.565–575.

Dyke, S.J., Spencer, B.F., Sain, M.K. and Carlson, J.D. (1997) 'Experimental study of magnetorheological dampers for seismic hazard mitigation', *Proceedings of the 1997 15th Structures Congress*, Portland, Oregon, Part 2, pp.1358–1362.

Dyke, S.J., Spencer, B.F., Sain, M.K. and Carlson, J.D. (1999) 'An experimental study of magnetorheological dampers for seismic hazard mitigation', *Proceedings of the 1999 Structures Congress*, New Orleans, Louisiana, pp.1358–1362.

Giuclea, M., Sireteanu, T., Stancioiu, D. and Stammers, C.W. (2004) 'Modeling of magnetorheological damper dynamic behavior by genetic algorithms based inverse method', *Proc. Romanian Academy*, Vol. 5, No. 1, pp.1–10.

Goodhew, I.C.B., Hutt, B.D. and Warwick, K. (2006) 'Control and experimentation of a personal robot tracking system', *Int. Journal of Modelling Identification and Control*, Vol. 1, No. 1, pp.4–12

Guo, D.L., Hu, H.Y. and Yi, J.Q. (2004) 'Neural network control for a semi-active vehicle suspension with a magnetorheological damper', *Journal of Vibration and Control*, Vol. 10, No. 3, pp.461–471.

Hong, K.S., Sohn, H.C. and Hedrick, J.K. (2002) 'Modified skyhook control of semi-active suspensions: a new model, gain scheduling and hardware in the loop tuning', *Journal of Dynamic Systems Measurement and Control*, Vol. 124, pp.158–167.

IMC (2002) *IMC-FAMOS User's Manual*, IMC GmbH., Berlin, Germany.

Inman, D.J. (1994) *Engineering Vibration*, Prentice-Hall, Englewood Cliffs, NJ.

Jalili, N. (2002) *Mechanical System Design Handbook (Chapter 12): Semi Active Suspension Systems*, CRC Press LLC, Boca Raton, Florida, USA.

Jansen, L.M. and Dyke, S.J. (1999) 'Investigation of nonlinear control strategies for the implementation of multiple magnetorheological dampers', *Proceedings of the 13th Engineering Mechanics Conference*, Reston, Virginia, pp.551–557.

Jansen, L.M. and Dyke, S.J. (2000) 'Semi active control strategies for MR dampers: a comparative study', *Journal of Engineering Mechanics*, ASCE, Vol. 126, No. 8, pp.795–803.

Kamath, G.M. and Wereley, N. (1997) 'Nonlinear viscoelastic-plastic mechanisms based model of an electrorheological damper', J*ournal of Guidance, Control Dynamics*, Vol. 20, pp.1125–1136.

Lam, H.F. and Liao, W.H. (2001) 'Semi-active control of automotive suspension systems with magnetorheological dampers', *Proceedings of SPIE-Smart Structure and Materials*, March 5–8, Newport Beach, CA, pp.125–136.

Liao, W. H. and Wang, D.H. (2003) 'Semiactive vibration control of train suspension systems via magnetorheological dampers', *Journal of Intelligent Material Systems and Structures*, Vol. 14, p.161.

Nishimura, H. and Kayama, R. (2002) 'Gain-scheduled control of a semi-active suspension using an MR damper', *Transactions of the Japan Society of Mechanical Engineers Part C*, Vol. 68, No. 12, pp.3644–3651.

Pang, L., Kamath, G.M. and Wereley, N.M. (1998) 'Dynamic characterisation and analysis of magnetorheological damper behaviour', *SPIE Conference on Passive Damping and Isolation*, SPIE, Vol. 3327, pp.284–302.

Raynal, W. (2003) 'Cadillac XLR', *Autoweek Magazine*, December.

Roschke, P.N. and Atray, V. (2002) *Neuro-Fuzzy Control of Vertical Vibrations in Railcar Using Magnetorheological Dampers*, Report No. 405450-00112, Association of American Railroads, Pueblo, CO.

Rui, L., Chen, W.M., Yu, M. and Liu, D.K. (2004) 'Fuzzy intelligent control of automotive vibration via magneto-rheological damper', *Proceedings of the 2004 IEEE Conference on Cybernetics and Intelligent Systems*, IEEE, December 1–3, Singapore, pp.503–507.

Scholz, P. (2000) *Á-MUSYCS User's Manual 2.0*, IMC GmbH, Berlin, Germany.

Schurter, K.C. and Roschke, P.N. (2000) 'Fuzzy modeling of a magnetorheological damper using ANFIS', *Proceedings of the 9th IEEE International Conference of Fuzzy System 2000*, San Antonio, Texas, Vol. 1, May 7–10, pp.122–127.

Schurter, K.C. and Roschke, P.N. (2000) 'Fuzzy modeling of a magnetorheological damper using ANFIS', *Proceedings of the 9th IEEE International Conference of Fuzzy System 2000*, San Antonio, Texas, Vol. 1, May 7–10, pp.122–127.

Sheng, Y., Wang, C. and Pan, Y. (2004) 'Semi-active control law for magnetorheological damper based on the linear quadratic Gaussian/loop transfer recovery method', *Journal of Engineering Mechanics*, Tsinghua University, Vol. 21, No. 1, pp.112–117.

Simon, T.M., Reitich, F., Jolly, M.R., Ito, K. and Banks, H.T. (2001) 'The effective magnetic properties of magnetorheological fluids', *Journal of Mathematical and Computer Modeling*, Vol. 33, pp.273–284.

Sireteanu, T., Stancioiu, D. and Stammers, C.W. (2004) 'Experimental assessment of a semi-active suspension with magnetorheological damper', *Proceedings of the 7th Biennial Conference on Engineering Systems Design and Analysis*, Manchester, UK, July 19–22, Vol. 1, pp.879–884.

Spencer, B.F., Dyke, S.J. and Deoskar, H.S. (1997) 'Benchmark problems in structural control, Part I: active mass driver system', *Proceedings of Structures Congress XV*, Portland, Oregon, pp.1267–1279.

Tang, C.Y., Zhang, T.X., Cao, W. and Zhou, W. (2009) 'Research on the control and simulation of vehicle suspension systems', *Int. Journal of Modelling Identification and Control*, Vol. 7, No. 1, pp.49–56.

Visnic, B. (2003) 'Spicy controversy: a review of the Porsche cayenne', *Ward's Auto World Magazine*, April.

Wang, E.R., Ma, X.Q., Rakheja, S. and Su, C.Y. (2005) 'Force tracking control of vehicle vibration with MR-damper', *Symposium on Intelligent Control*, Limassol, Cyprus, June 27–29.

Wereley, N.M., Pang, L. and Kamath, G.M., (1998) 'Idealized hysteresis modeling of electrorheological and magnetorheological dampers', *Journal of Intelligent Material System Structure*, Vol. 9, pp.642–649.

Yiming, R. and Xiangying, B. (2004) 'An automobile semi-active suspension system using neural network control and simulation', P*roceedings – 2004 International Conference on Intelligent Mechatronics and Automation*, August 26–31, Chengdu, China, pp.187–190.

Yokoyama, M., Hedrick, J.K. and Toyama, S. (2001) 'A model following sliding mode controller for semi-active suspension systems with MR dampers', *Proceedings of the American Control Conference*, Arlington, VA, Vol. 4, June 25–27, pp.2652–2657.

Zapateiro, M., Luo, N. and Karimi, H. R. (2009) 'Semiactive control of a base isolated building using magnetorheological dampers', *Int. Journal of Modelling Identification and Control*, Vol. 7, No. 1, pp. 41-48.

Zhang, X., Yue, W. and Chen, L. (2004) 'Application of fuzzy control on damping coefficient in vehicle semi-active suspension', *Transactions of the Chinese Society of Agricultural Machinery*, Vol. 35, No. 2, pp.5–17.